Drug uptake, lipid rafts and vesicle trafficking modulate resistance to an anticancer lysophosphatidylcholine analogue in yeast

Alvaro Cuesta-Marbán[1], Javier Botet[2*], Ola Czyz[3], Luis M. Cacharro[1], Consuelo Gajate[1], Valentín Hornillos[4], Javier Delgado[4], Hui Zhang[1**], Francisco Amat-Guerri[4], A. Ulises Acuña[5], Christopher R. McMaster[6], Jose Luis Revuelta[2], Vanina Zaremberg[3] and Faustino Mollinedo[1]

[1]*Instituto de Biología Molecular y Celular del Cáncer, Centro de Investigación del Cáncer, CSIC-Universidad de Salamanca, Campus Miguel de Unamuno, E-37007 Salamanca, Spain*

[2]*Departamento de Microbiología y Genética, Universidad de Salamanca, Campus Miguel de Unamuno, E-37007 Salamanca, Spain*

[3]*Department of Biological Sciences, University of Calgary, 2500 University Dr, NW, Calgary, Alberta, T2N 1N4, Canada.*

[4]*Instituto de Química Orgánica General, CSIC, Juan de la Cierva 3, E-28006 Madrid, Spain*

[5]*Instituto de Química Física Rocasolano, CSIC, Serrano 119, E-28006 Madrid, Spain*

[6] *Department of Pharmacology, Atlantic Research Centre, Dalhousie University, Halifax, Nova Scotia, B3H 4R2, Canada*

Running title: Rafts and vesicle traffic in antitumor lipid resistance

Keywords: chemogenomic screen, ether lipids, lysophosphatidylcholine analogues, lipid rafts, ESCRT, retrograde transport, *Saccharomyces cerevisiae*

To whom correspondence should be addressed:
Faustino Mollinedo, Instituto de Biología Molecular y Celular del Cáncer, Centro de Investigación del Cáncer, CSIC-Universidad de Salamanca, Campus Miguel de Unamuno, E-37007 Salamanca, Spain. Phone: (+34) 923-294806, Fax: (+34) 923-294795, E-mail: fmollin@usal.es
or
Vanina Zaremberg, Department of Biological Sciences, University of Calgary, 2500 University Dr, NW, Calgary, AB, T2N 1N4, Canada. Phone (403) 220-4298, Fax: (403) 289-9311, E-mail: vzarembe@ucalgary.ca

*Present address: Instituto de Biología Funcional y Genómica (IBFG), CSIC-Universidad de Salamanca, E-37007 Salamanca, Spain.
**Present address: Department of Chemistry and Life Science, Xiangnan University, Chenzhou 423000, Hunan, P.R. China.

Background: The antitumor lipid edelfosine kills yeast by inducing selective internalization of raft-associated proteins.
Results: Impairing vesicular trafficking to the vacuole counteracted edelfosine-induced plasma membrane alterations without affecting internalization of the drug.
Conclusion: Recycling of raft-associated proteins to the plasma membrane prevents edelfosine cytotoxicity.
Significance: Vesicular trafficking is a critical process mediating edelfosine resistance in yeast that could be extrapolated to tumor cells.

The ether-phospholipid edelfosine, a prototype antitumor lipid

(ATL), kills yeast cells and selectively kills several cancer cell types. To gain insight into its mechanism of action, we performed chemogenomic screens in the *Saccharomyces cerevisiae* gene-deletion strain collection, identifying edelfosine-resistant mutants. *LEM3, AGP2* and *DOC1* genes were required for drug uptake. Edelfosine displaced the essential proton pump Pma1p from rafts, inducing its internalization into the vacuole. Additional ATLs, including miltefosine and perifosine also displaced Pma1p from rafts to the vacuole, suggesting that this process is a major hallmark of ATL cytotoxicity in yeast. Radioactive and synthetic fluorescent edelfosine analogues accumulated in yeast plasma membrane rafts and subsequently the endoplasmic reticulum. Although both edelfosine and Pma1p were initially located at membrane rafts, internalization of the drug towards endoplasmic reticulum and Pma1p to the vacuole followed different routes. Drug internalization was not dependent on endocytosis and was not critical for yeast cytotoxicity. However, mutants affecting endocytosis, vesicle sorting or trafficking to the vacuole including the retromer and ESCRT complexes, prevented Pma1p internalization and were edelfosine-resistant. Our data suggest that edelfosine-induced cytotoxicity involves raft reorganization, and retromer- and ESCRT-mediated vesicular transport and degradation of essential raft proteins leading to cell death. Cytotoxicity of ATLs is mainly dependent on the changes they induce in plasma membrane raft-located proteins that lead to their internalization and subsequent degradation. Edelfosine toxicity can be circumvented by inactivating genes that then result in the recycling of internalized cell-surface proteins back to the plasma membrane.

Synthetic ether-linked analogues of phosphatidylcholine and lysophosphatidylcholine, collectively named alkyl-lysophospholipid analogues (ALPs) or synthetic antitumor lipids (ATLs) (1,2), constitute a family of promising anticancer compounds. Unlike most chemotherapeutic drugs ATLs do not target DNA but instead act at the level of the cell membrane (1-3). Major academic and pharmaceutical interest in the antitumor mechanisms of ATLs has been rekindled by the observation that the prototype ATL edelfosine (1-*O*-octadecyl-2-*O*-methyl-*rac*-glycero-3-phosphocholine; ET-18-OCH_3) (Fig. 1) selectively induces apoptosis in cancer cells (4,5), mainly due to preferential drug uptake by tumor cells (4-6). Edelfosine is the most potent pro-apoptotic ATL (7-10). Edelfosine-induced apoptosis in hematopoietic cancer cells involves accumulation of the drug in lipid rafts (4,8,11,12), which results in recruitment and clustering of Fas/CD95 death receptor into rafts, intracellular activation of the death receptor pathway, and apoptosis (4,7,8,12,13). Furthermore, edelfosine accumulates in the endoplasmic reticulum (ER), promoting an ER stress response and apoptosis in solid tumor cells (10,14,15). Recent *in vivo* assays highlight the antitumor activity of edelfosine in animal models for a number of hematological malignancies (8,9) and solid tumors (10).

A major problem in the treatment of cancer is the development of drug resistance. Understanding the molecular mechanisms involved in the generation of resistant phenotypes is critical in trying to overcome drug resistance and to improve current therapy. The antitumor activity of another ATL, perifosine (octadecyl (1,1-dimethyl-piperidino-4-yl)-phosphate, D-21266; Fig. 1), is being tested in ongoing clinical trials; and miltefosine (Fig. 1) is used in the clinic as a palliative treatment for cutaneous metastases from breast cancer (16). Gaining insight into the mechanisms of action of ATLs, as well as in the identification of the molecular processes that lead to drug resistant and sensitive phenotypes, is of major importance for the clinical development of these synthetic compounds.

Edelfosine is cytotoxic against the budding yeast *Saccharomyces cerevisiae* (17), although the underlying mechanism is not fully understood. The yeast flippase subunit Lem3p has been shown to be essential for drug uptake (18), and we have previously found that edelfosine displaces the essential H^+-pump Pma1p from plasma membrane microdomains, resulting in its degradation (17). *S. cerevisiae* is a useful tool for identifying human drug targets and modulators of drug activity (19). Comparison

of the yeast and human genomes has revealed that 30% of known genes involved in human disease have yeast orthologs, and a large number of yeast genes exhibit a link to human disease genes (20,21). In this study, and the accompanying paper (Czyz *et al.*), we performed a chemical-genetic screen *versus* the deletion strain set and identified genes that led to either increased edelfosine resistance or sensitivity. We also synthesized a set of fluorescent edelfosine analogues that retained the properties of the parent compound and allowed its subcellular localization to be determined.

By combining genetic and functional approaches, we unveiled a novel mechanism of action in the killing of *S. cerevisiae* that may be extrapolative to tumor cells. In addition to the identification of three genes required for edelfosine uptake our data indicate that edelfosine accumulates in lipid rafts and ER in *S. cerevisiae*, and mediates its cytotoxic activity by affecting raft protein composition which eventually leads to intracellular acidification (see accompanying paper, Czyz *et al.*). This alteration in raft composition seems to be conserved within the ATL family, as it was also observed for miltefosine and perifosine. The selective displacement of crucial proteins from lipid rafts results in their endosome-mediated transport to the vacuole, where they undergo degradation. The end result is an alteration in intracellular pH that eventually leads to cell death. The yeast genome-wide screen and subsequent experiments performed here revealed that vesicular trafficking is a critical process mediating edelfosine resistance, with mutants that result in increased recycling between endosomal compartments and the plasma membrane being resistant to edelfosine cytoxocity. This is a highly conserved process and thus this mode of resistance may be extrapolatable from yeast to tumor cells.

EXPERIMENTAL PROCEDURES

Yeast strains, plasmids and growth conditions

The collection of nonessential haploid yeast deletion strains derived from parental strain BY4741 (MAT **a** *his3Δ1 leu2Δ0 met15Δ0 ura3Δ0*) was obtained from Euroscarf. All other strains used in this study are listed in Table 1. The endoplasmic reticulum marker encoded by *ELO3* was subcloned into the pUG35 (*URA3*) vector (22) using EcoR1 and Sal1 restriction enzyme sites, in frame with green fluorescent protein (GFP) coding sequence at its 3' end. The YCplac111-*SEC63*-GFP (*SEC63*-GFP under control of *SEC63* promoter into *CEN/LEU2* vector) was kindly provided by Symeon Siniossoglou (University of Cambridge, UK) (23). The centromeric plasmid used to express Pma1p-GFP (in pRS316, *URA3*) was kindly provided by Annick M. Breton (Institut de Biochimie et Génétique Cellulaires, France) (24). The centromeric vector YCplac111 (Stratagene) was used to express the *VPS29* and *VPS35* genes in their respective *vps29*Δ and *vps35*Δ knockout strains. Red fluorescent protein (RFP) tagged marker strains (25) for the indicated organelles and cellular structures (kindly provided by Peter Arvidson, Harvard, USA) were used to examine the subcellular location of fluorescent edelfosine.

Yeast strains were grown on standard rich medium YPD (1% yeast extract, 2% Bacto-peptone, 2% glucose), synthetic minimal medium (SD; 0.17% yeast nitrogen base without amino acids, 2% glucose and supplements according to the requirements of the strains), and synthetic complete medium (SC; SD medium with 0.079% complete supplement mixture (ForMedium, Norwich, UK). Agar (2%) was added for solid plates. Unless otherwise indicated all yeast cultures were incubated at 28°C.

Growth of cells treated with edelfosine was monitored by optical density at a wavelength of 595 nm (OD_{595}). A preculture was grown overnight in YPD to log-phase. A volume of 2 ml of fresh YPD was then inoculated to an OD_{595} of 0.3 and immediately treated with edelfosine. Cells were incubated for 24 h and sample aliquots were taken at the designated times to measure absorbance. Edelfosine was routinely used at 15 μM for treatment in liquid medium unless otherwise indicated.

Large-scale edelfosine resistance screens

The haploid deletion collection in the BY4741 background was screened for resistance to edelfosine in SC liquid medium. Strains were pinned from 96-well frozen stock plates by using a stainless steel 96-pin replicator (Nalgene Nunc International) into 96-well plates containing 150 μl of liquid

YPD medium supplemented with G418 (150 mg/l; Gibco-BRL). The plates were incubated at 28°C for 3 days and then pin replicated onto liquid SC in 96-well plates containing either no drug or 60 µM edefosine. Plates were incubated at 28°C and growth was quantitatively scored every 24 h over a period of 7 days by optical density readings at OD_{595} using a microplate spectrophotometer (model 550; Bio-Rad Laboratories). Edelfosine resistance was scored on the basis of the relative growth of each mutant against that of the wild-type strain in the same plate and with that of each mutant strain in plates where no drug was added. Putative edelfosine-resistant strains identified during the screening of the yeast knockout collection were further retested at least in duplicate under the same conditions described for the screen. Gene deletion strains that consistently grew at or above a 4-fold higher rate than wild-type cells in the presence of 60 µM edelfosine for 72 h in five independent screening assays were considered drug-resistant. These cutoff conditions led to reliable and highly reproducible results. Selected resistant strains were retested again from the original haploid deletion collection stock for drug resistance, using 60 µM edelfosine, to minimize those arising due to second site mutations accumulating in other regions of the genome during drug exposure.

Growth of resistant strains was further confirmed in solid medium. Cultures grown in 96-well plates were resuspended using a 96-well plate shaker (Microtec; Infors AG), and four serial 10-fold dilutions in water were done. Five-microliter aliquots of the diluted cultures were spotted using a replica plater for a 96-well plate (Sigma-Aldrich) to OmniTray plates (Nalgene Nunc International) containing SC solid medium, to which edelfosine was added once the medium had cooled to ~50ºC. The plates were incubated at 28°C for 3 days and analyzed for cell growth every 24 h.

*Data analysis and functional group classificatio*n

To identify functional clusters of genes statistical analysis of overrepresentation of functional categories affected by edelfosine was performed by using Gene Ontology (GO) (26), functional annotations tools from FatiGo, FunSpec (http://funspec.med.utoronto.ca/) (27), the GO term finder at the *Saccharomyces* Genome Database (SGD) (http://www.yeastgenome.org/) (28), and the MIPS functional catalogue (http://mips.gsf.de/genre/proj/yeast). Gene classification was done subjectively with reliance on the *Saccharomyces* Genome Database (SGD), the Yeast Proteome Database, the Comprehensive Yeast Genome Database at MIPS and the literature.

Edelfosine uptake in yeast mutants

[^{3}H]edelfosine uptake was analyzed in the 91 yeast mutants that showed the highest drug resistance (Supplementary Table S1), as described (7) with slight modifications. [^{3}H]edelfosine (specific activity, 42 Ci/mmol) was synthesized by Amersham Buchler, Braunschweig, Germany. Briefly, the mutants were incubated at 28^{o}C to late exponential phase in 1 ml of YPD in a 96-well microtiter plate. The OD_{595nm} of each well was measured to ensure the same amount of cells from each mutant was present per well. [^{3}H]edelfosine (60 µM and 2 x 10^4 cpm per well) was added and the cells were incubated at 28^{o}C at 800 rpm for 1 h. The non-incorporated [^{3}H]edelfosine was washed-out from the culture by exhaustive washing (5 times) with 1 ml of 3% bovine serum albumin (BSA) in phosphate buffered saline (PBS). Washed cells were resuspended in 500 µl of PBS and mixed with 1.5 ml of scintillation liquid. The radioactivity incorporated into cells was measured in a Beckman liquid scintillation counter. The uptake assay was carried out three times (data for each mutant strain was calculated from three independent biological replicates). Deletion mutants with reduced edelfosine uptake were complemented with the corresponding wild type genes expressed from a centromeric plasmid (pRS416), and drug uptake was assayed as above.

Detergent-resistant membrane isolation and western blots

Yeast detergent-resistant membranes (DRM) were isolated as described (17) from total crude membranes. Yeast cells were grown to mid-log phase, and an amount of cells equivalent to 50 OD_{595} units was untreated or incubated in the presence of 15 µM edelfosine for the indicated times. Cells were then washed three times with PBS and

once with 1 M sorbitol containing 10 mM NaN_3 and 10 mM NaF. The cell pellet was stored at -20 °C. Cells were resuspended in 350 µl of TNE buffer (50 mM Tris-HCl, pH 7.4, 150 mM NaCl, and 5 mM EDTA, 20 µg/ml leupeptin, 20 µg/ml aprotinin, 1 mM phenylmethylsulfonyl fluoride, and protease inhibitor mixture (Roche)), and broken with the aid of Fastprep (four 15-s pulses, 5.5 speed) in the presence of glass beads at 4°C. Unbroken cells were removed by a 500 x *g* spin for 5 min at 4°C, and the resulting supernatant (total cell lysate) was centrifuged for 3 h at 4°C in an SW40 rotor at 35,000 rpm (218,000 x *g*) to pellet crude cellular membranes. The pellet was resuspended in Mes-buffered saline (MBS; 25 mM Mes, pH 6.5, 150 mM NaCl) including 60% sucrose, and Triton X-100 was added to a final concentration of 1%. After 1 h at 4°C, membranes were further disrupted with several strokes in a Potter-Elvehjem tissue grinder and 350 µl of the extracted membranes were mixed with 2.27 ml of 60% sucrose in MBS. This was placed at the bottom of an ultracentrifuge tube and overlaid with a sucrose step gradient from 5 to 50% sucrose in MBS (0.89 ml at 5%, 0.89 ml at 30%, 1.78 ml at 40%, 1.78 ml at 45%, and 3.54 ml at 50%). Sucrose gradients were centrifuged in an SW40 rotor at 38,000 rpm (257,000 x *g*) for 18 h at 4°C in a Beckman Optima LE-80K ultracentrifuge and 1-ml fractions were collected from the top of the gradient. For each fraction, 20 µl was subjected to SDS-PAGE, immunoblotting, and enhanced chemiluminescence detection.

For incorporation of edelfosine into DRMs, cells were incubated with 15 µM [^{3}H]edelfosine (5.3 x 10^5 dpm/mol) for the indicated times and subjected to lipid raft isolation as above.

DRM isolation from yeast treated with edelfosine (Inkeysa and Medmark), miltefosine (Cayman Chem) and perifosine (Aeterna Zentaris) was also performed as indicated in the accompanying paper (*Czyz et al.*) using Optiprep gradients. Densitometry was performed using Image J (Wayne Rasband, National Institutes of Health, USA). Experiments were done at least three times.

For western blot analysis, proteins were transferred to polyvinylidene difluoride membranes (PVDF) (GE Healthcare, Little Chalfont, Buckinghamshire, UK), and blots were incubated with antibodies to Pma1p and Gas1p (kind gifts of Ramón Serrano, Universidad Politécnica de Valencia, Spain, and Howard Riezman, University of Geneva, Switzerland, respectively), and subsequently with horseradish peroxidase-conjugated secondary antibodies followed by detection using enhanced chemiluminescence.

Edelfosine fluorescent analogues

Fluorescent analogues of edelfosine (Fig. 1A) were synthesized in a way in which the physico-chemical properties and biological activity of the parent drug remained essentially unperturbed. We designed synthetic strategies that allowed precise control of the changes introduced in the structure and properties of the parent drug to produce *de novo* fluorescent bioactive analogues of the alkyl-lipid. Synthesis of the fluorescent analogues of edelfosine used in this study, namely containing the conjugated *all-(E)*-phenyltetraene or *all-(E)*-phenyltrienyne blue-emitting chromophores (PTE-ET and PTRI-ET, respectively; Figure 1), and a 2-substituted borondifluorodipirromethene group (BODIPY or BDP) attached to and aligned with the alkyl chain of the ether-lipid (green-emitting Et-BDP-ET and Yn-BDP-ET; Figure 1) has been detailed elsewhere (4,29,30). Spectral features of the distinct fluorescent edelfosine analogues used in this study have been previously described (4,29,30). The filters used to examine the PTE-ET and PTRI-ET analogues were those for DAPI staining (BP 546 FT 580 LP 590). The filters to examine the BDP-ET analogues were those corresponding for GFP (41017 HQ 470/40X Q495LP HQ525/50).

Microscopy

Both Nomarski interference contrast, light, and fluorescence microscopy were used to visualize different subcellular organelles and proteins as well to examine the localization and effect on the cell of edelfosine. Images were obtained using a Carl Zeiss Axioplan 2 microscope. Images were acquired using Openlab software (PerkinElmer).

Drug localization was monitored with fluorescent analogues of edelfosine that were added directly to 1 ml of log-phase cultures in

YPD. Cells were incubated in darkness for 30 min, washed, applied directly to the slide and immediately imaged. PTE-ET and PTRI-ET were added at a final concentration of 15 μM, and due to their proneness to undergo photobleaching, pictures were taken as soon as the samples were exposed to ultraviolet light. Et-BDP-ET and Yn-BDP-ET, which have a more intense and resilient fluorescence, were added at a final concentration of 5 μM and could be imaged normally. Images of other fluorescent markers were always taken after the analogues were imaged. For studies of drug internalization the soluble salt Lucifer yellow (LY, Sigma) and the lypophilic dye FM 4-64 (Biotium) were simultaneously used as endocytosis markers. Cells were preincubated for 1 h, at either 4ºC or 30ºC, in the presence of 2.5 mg/ml LY and 10 μM FM 4-64. Cells were washed, resuspended in YPD and subsequently incubated for 15 min (or 1 h for 0ºC) with 15 μM PTE-ET, while keeping the previous temperature, and imaged immediately afterwards.

Pma1p internalization was monitored using strains transformed with a GFP-tagged form. Various strains were transformed with either a vector carrying the fusion protein or an empty one. Cells were grown to early log phase (OD_{595}=0.2) and preloaded with 10 μM FM4-64 for 45 min. Cells were washed, resuspended in the same volume of medium and treated with 15 μM edelfosine. After a 4 hr incubation cells were harvested and imaged.

Statistical analysis

Values are expressed as a mean ± SD with the number of experiments indicated.

RESULTS

Cytotoxic activity of edelfosine in S. cerevisiae

In order to set the conditions for chemogenomic screens, we first determined the minimal concentration necessary to inhibit growth of wild-type *S. cerevisiae* strains in liquid culture. Yeast lacking Lem3p (*lem3*Δ), which have been reported to be resistant to edelfosine (18), were used as a positive control of growth inhibition. We also included yeast mutants lacking Dnf2p and Drs2p, two phospholipid translocases (flippases) involved in lipid and endocytic trafficking (31). Lem3p is an activator of Dnf2p and other members of the phospholipid translocase family. Dnf2p is a plasma membrane phospholipid and lysophospholipid translocase that can use edelfosine as a substrate, while Drs2p is a trans-Golgi localized phospholipid translocase that affects vesicular trafficking. Edelfosine inhibited wild type yeast growth at 15 μM, while the *lem3*Δ strain was resistant to edelfosine even at 70 μM (Fig. 2a). The *dnf2*Δ and *drs2*Δ strains showed an intermediate phenotype with growth inhibition at 35 μM and 17.5 μM, respectively, probably due to partial functional redundancy among them and additional members of this protein family (32).

Identification of edelfosine-resistant mutants in S. cerevisiae

Next, we performed large-scale chemical-genomic screens using a haploid collection of *S. cerevisiae* deletion mutants, individually deleted for non-essential genes (~4,800 genes) to test for enhanced resistance to edelfosine compared to wild-type cells. Strains that grew in liquid culture at a rate ≥4-fold that of wild-type cells in the presence of 60 μM edelfosine for 72 h in five independent screening assays were considered drug-resistant (Fig. 2b). These cutoff conditions led to highly reproducible results. From these screens we identified 262 genes whose inactivation conferred resistance to edelfosine in *S. cerevisiae* (Table 1, and Supplementary Table S1). Functional analysis of these genes revealed the enrichment of statistically significant clusters of biological processes involved in edelfosine resistance. This analysis identified genes involved in vesicular transport (including ESCRT and retromer complexes), protein biosynthesis, and mitochondrial processes (Fig. 2c, Table 2, and Supplementary Table S1). Table 2 shows some of the most relevant genes involved in edelfosine resistance regarding vesicular traffic and drug uptake. The resistant mutants were significantly enriched in endosome- and mitochondria- localized proteins. In this work we focused on the mechanism of resistance conferred by mutants in the endosomal trafficking pathways.

Mutant strains involved in edelfosine uptake

Because edelfosine must be incorporated by the target cell to exert its cytotoxic effect (4,5), we examined whether the edelfosine resistance of the selected strains was due to deficient drug uptake. [^{3}H]edelfosine uptake was analyzed in the 91 yeast mutants that showed the highest drug resistance (Supplementary Table S1) and only *lem3*Δ, *agp2*Δ and *doc1*Δ mutants resulted in drug uptake deficiency (Fig. 2d). This phenotype was reverted by transformation of each mutant with the corresponding wild-type gene (Fig. 2d). It has been previously demonstrated that inactivation of *LEM3* blocked edelfosine uptake (18). Interestingly, our data indicated that the L-carnitine and bleomycin transporter Agp2p (33,34), and Doc1p, which is involved in ubiquitination of the anaphase promoting complex (APC), were also involved in edelfosine uptake (Fig. 2d). These results indicate that resistance to edelfosine in the majority of mutants identified in our screen is not due to reduced uptake of the drug.

Fluorescent analogues of edelfosine and drug localization to the plasma membrane and ER

Because the uptake of edelfosine is critical for its cytotoxic action in yeast we examined its localization in *S. cerevisiae*. To do so we used a first generation of fluorescent edelfosine analogues, tagged with UV-absorbing *all-(E)*-phenyltetraene or *all-(E)*-phenyltrienyne blue-emitting chromophores (PTE-ET and PTRI-ET, respectively) (Fig. 1), and a second generation of fluorescent analogues where a 2-substituted borondifluorodipirromethene group (BODIPY or BDP) was attached to and aligned with the alkyl chain of the ether-lipid yielding green-emitting Et-BDP-ET and Yn-BDP-ET analogues (Fig. 1) (4,29,30). Absorption and emission spectra in the visible wavelength range, enhanced fluorescence yield and higher resistance to photodegradation of the latter analogues improved the lateral resolution of living-cell imaging techniques and extended the recording time (30).

The above fluorescent analogues preserved the anticancer activity of the parent drug, PTE-ET showing the highest killing activity (4,15,30). Likewise, similar actions of the above fluorescent compounds were found in yeast, with PTE-ET being the most effective fluorescent analogue in inhibiting yeast growth (*data not shown*). In addition, similarly to what was observed with radioactive edelfosine (Fig. 2d), no uptake of any of the fluorescent edelfosine analogues was detected in *lem3*Δ mutants as compared to wild-type yeast (Fig. 3). These data suggest that the above fluorescent edelfosine analogues behave as *bona fide* analogues to analyze edelfosine localization in yeast. We found that all of the emitting edelfosine analogues yielded a similar localization pattern in yeast (Fig. 3) corresponding to a bag-like envelope surrounding the nucleus, (visualized by the nuclear marker Sik1p-RFP), which resembled the morphological traits of ER (Fig. 4). On these grounds, PTE-ET was used hereafter.

Using GFP-tagged markers for distinct subcellular organelles, we found that PTE-ET was mainly localized to the ER, as assessed by using Elo3p-GFP as an ER marker (Figs. 4, 5 and 6a). We found good co-localization between PTE-ET and Elo3p-GFP (Figs. 4, 5 and 6a), whereas no co-localization was observed with markers for other subcellular structures and compartments including Golgi (Anp1p, Chc1p), spindle pole (Spc42p), endosomes (Snf7p), cytoskeleton (Sac6p), peroxisomes (Pex3p) and lipid droplets (Erg6p) (data not shown). Further confirmation of the ER location of edelfosine was found by co-localization of PTE-ET fluorescent analogue with the ER marker Sec63p (Fig. 5). These data suggest that fluorescent edelfosine analogues are incorporated into the PM and transit to the ER.

ER localization of edelfosine is not dependent on endocytosis

One of the largest clusters of edelfosine-resistant mutants comprised strains defective in endocytosis. We examined the putative involvement of endocytosis in the ER localization of edelfosine. Inactivation of either *END3* or *END4* leads to defects in endocytosis (35). Our chemogenomic screen identified *end3*Δ as edelfosine resistant in addition to endocytosis-related mutants with inactivated *MYO5*, *LDB17* or *RHO4* genes (Table 1). However, PTE-ET was still ER localized in the *end4 pep4*Δ mutant and wild-type cells (incubated at 4ºC to slow down the rate of endocytosis) (Fig. 6b). In both cases,

inhibition of endocytosis was confirmed by a decrease or block in the uptake of the soluble endocytosis marker Lucifer yellow and the lipophilic marker FM4-64 (Fig. 6b).

These results show that endocytosis does not play a role in the ER location of edelfosine. Furthermore, because the *end4 pep4*Δ mutant is edelfosine-resistant (17), drug localization to the ER is not critical for its cytotoxicity.

Pma1p internalization, lipid rafts and endocytosis in ATL-mediated cytotoxic activity

Because the above data suggested that inhibition of endocytosis prevented cell death, but was not crucial for edelfosine intracellular localization, we hypothesized that an essential step for edelfosine toxicity could be the internalization of certain membrane proteins by endocytosis. We have previously shown that edelfosine accumulates in plasma membrane lipid rafts in *S. cerevisiae* displacing Pma1p from these membrane microdomains resulting in Pma1p transit to the vacuole (17). In this regard, we found that incubation of yeast at 4ºC abrogated internalization of GFP-tagged Pma1p following edelfosine treatment, but not the intracellular location of edelfosine (Figs. 6b and 6c).

We went on to analyze displacement of proteins from lipid rafts by edelfosine. The 100-kDa yeast lipid raft protein Pma1p was mainly located in fractions 4-6 of the sucrose gradient of untreated *S. cerevisisae*, thus identifying the raft-enriched fractions (Fig. 7a, *inset*). As shown in Fig. 7a, we found that edelfosine was mainly located in non-raft fractions at early time points, but became enriched in rafts at longer incubation times. Interestingly, edelfosine accumulation in rafts was accompanied by Pma1p displacement from these membrane domains (Figs. 7a and 7b), which was followed by its internalization and degradation in the vacuole (17). However, the glycosylphosphatidylinositol (GPI) anchored protein Gas1p, another lipid raft protein, was not displaced from rafts (Fig. 7b). This Pma1p displacement from rafts was blocked in the *end4 pep4*Δ mutant (Fig. 7b), despite the fact that this mutant accumulated large amounts of edelfosine in lipid rafts (Fig. 7a) and drug internalization was not prevented (Fig. 6b). Altogether, these results suggest that edelfosine and Pma1p are delivered to the interior of the cell through distinct mechanisms. Thus, Pma1p internalization is mediated by endocytosis, whereas edelfosine internalization is endocytosis-independent. In addition, it is interesting to note that most of the edelfosine was visualized intracellularly in the ER after 3 h of incubation, while a significant amount of the drug was also found in lipid rafts (*data not shown*), suggesting the presence of rafts in the ER. This notion is further supported by the high proportion of edelfosine in rafts in *end4 pep4*Δ mutant, while being visualized in the ER by fluorescence microscopy (cf. Figs. 6b and 7a). Presumably, resistance in the *end4 pep4*Δ mutant comes from a downstream effect in the mechanism of drug toxicity; that is, uptake of the drug and its translocation to the ER continues, but Pma1p endocytosis/degradation is impaired.

We also found that, like edelfosine, the other clinically relevant ATLs miltefosine and perifosine were able to induce Pma1p displacement from lipid rafts and subsequent internalization into the vacuole in yeast, as assessed by detergent-resistant membrane isolation (Figs. 8a and 8b) and fluorescence microscopy (Fig. 8c). In contrast, treatment of yeast with non-ATL compounds including cycloheximide, brefeldin A or hygromycin B, did not promote Pma1p displacement from plasma membrane rafts (*data not shown*). Thus, Pma1p displacement from rafts seems to be a general feature of ATL action, and not a general process occurring under drug-induced stress.

Involvement of vesicle-mediated transport in edelfosine resistance

A major cluster of edelfosine-resistant mutants included genes that mediated vesicular trafficking (Table 2, Supplementary Table S1, and Fig. 2c). A significant number of these genes are engaged in protein sorting at late endosomes, a process that seems to act as a major determinant for resistance to edelfosine.

Multiple pathways mediate recycling of internalized cell-surface proteins from endosomes back to the PM. Sorting of proteins at endosomes is a critical step for recycling. Sorting of proteins can be carried out by different protein complexes including sorting nexins, retromer complex and ESCRT

complex (36). Mutants in all of these pathways were identified in our screen.

We found that deletion of 4 out of the 5 components (*VPS35, VPS29, VPS26/PEP8* and *VPS17*) of the retromer, a highly conserved protein complex that mediates recycling to the PM as well as retrograde transport to the *trans*-Golgi network (TGN) (37), resulted in edelfosine resistance (Table 2). Drug resistance was also observed in mutants for the sorting nexins *SNX4* and *SNX42* (Table 2), which participate in an alternate retrograde transport mechanism (38). Deletion of the proteases *KEX1* or *KEX2*, involved in processing cargo proteins, also caused drug resistance (Table 2). *RAB7* has a role in retromer recruitment to endosomes in human cells (39), and deletion of its functional homolog in yeast *YPT7* caused edelfosine resistance (Table 2). Deletion of two components (*VPS52* and *VPS54*) of the **G**olgi-**A**ssociated **R**etrograde **P**rotein complex (GARP) (40) and the only non-essential member of the SNARE complex, *TLG2*, or the palmitoyltransferase *SWF1* required for Tlg1p stability involved in vesicle fusion to the TGN, also led to edelfosine resistance (Table 2).

We examined whether retrograde transport was required for the localization of edelfosine to the ER. To this aim we used the two most edelfosine-resistant strains with deletion in retromer genes, namely *vps29*Δ and *vps35*Δ. The involvement of the retromer in edelfosine cytotoxicity was confirmed by showing that *vps29*Δ and *vps35*Δ mutants restored the edelfosine-sensitivity phenotype when they were transformed with a centromeric plasmid containing their cognate *VPS29* or *VPS35* genes (Fig. 9). Next, we found that ER location of edelfosine was not affected in the *vps29*Δ and *vps35*Δ mutants (Fig. 10a). PTE-ET localized to the ER in the above deletion mutants, as assessed by using the ER-specific marker Elo3p-GFP, indicating that drug accumulation in the ER is independent of retrograde transport. However, Pma1p remained largely at the plasma membrane in these retromer mutants following exposure to edelfosine, as shown by fluorescence microscopy with a Pma1p-GFP fusion protein (Fig. 10b). These data further support that a critical step in edelfosine cytotoxicity is displacement of Pma1p from lipid rafts for subsequent degradation by the vacuole, and not accumulation of edelfosine in the ER.

In addition, our chemogenomic screen identified 11 of the 18 known members of ESCRT complexes as genes whose inactivation results in edelfosine resistance (complex 0: *VPS27*; complex I: *VPS23/STP22, VPS37/SRN2*; complex III: *DID4/VPS2, VPS24, VPS20*; ESCRT III-related proteins: *DID2* and *VPS4*; and proteins associated with ESCRT function: *DOA4*, *UBP2* and *BRO1*) (Table 2). The ESCRT complexes comprise sequential steps in the internalization of the early endosome membrane to form intraluminal vesicles (ILV). As the endosome matures it becomes a multivesicular body (MVB). Proteins targeted to the endosome membrane can be recycled or sorted to the MVB that then deliver the ILVs to the vacuole (yeast equivalent of the lysosome), where proteins are eventually degraded.

The edelfosine-resistant gene *DOA4* is an ubiquitin isopeptidase required for recycling ubiquitin from late endosomes and is essential for the maintenance of the free ubiquitin pool. Ubiquitination of proteins is a major determinant in their recognition by the ESCRT complex and subsequent vacuole-mediated degradation (41). In fact, genes coding for the E3 ubiquitin ligase protein adaptors *BUL2* and *BSD2* were also identified in our screen (Supplementary Table S1). In agreement with these findings, we show in the accompanying paper (Czyz *et al.*) that edelfosine indeed induces ubiquitination and internalization of not only Pma1p, but also nutrient H^+ symporters like the arginine transporter Can1p and uracil transporter Fur4p.

Yeast strains defective in retrograde transport still deliver edelfosine to the ER, however, a higher proportion of Pma1p is found at the PM in retromer mutants. This implies that recycling of Pma1p, and possibly other lipid raft associated proteins, confers edelfosine resistance.

DISCUSSION

ATLs such as edelfosine have shown promise for cancer treatment, but it has been difficult to further optimize their efficacy as the mechanism of action of these drugs remains to be fully elucidated. In this study

we present the first chemogenomic screen undertaken to uncover the underlying genetic mechanisms that mediate edelfosine resistance in yeast. The most powerful aspect of carrying out genetic screens is that the approach allows identification of unsuspected pathways that modulate cell sensitivity and resistance to the drug. We had previously determined that edelfosine disrupts lateral organization of the plasma membrane as an early event in its mode of action in yeast (17). In this study and the accompanying paper (Czyz *et al.*), we have found that following interaction of edelfosine with lipid rafts, resistance and sensitivity to this drug is mediated through two major processes, namely: i) disturbance of pH homeostasis (Czyz *et al.*); and ii) sorting of specific proteins at the endosome via sorting nexins and retromer at early and late endosomes, respectively and by the ESCRT vesicular trafficking pathway.

Based on the results reported here and the accompanying paper (Czyz *et al.*), we propose a working model for edelfosine-mediated cytotoxicity in yeast that involves lipid raft reorganization (Fig. 11, a-d) and loss of pH homeostasis (Fig. 11e), leading to cell death. Loss of lateral organization in the yeast plasma membrane is expected to impact a number of proteins that use lipid microdomains as scaffolds to modulate their activity/function. Despite the fact that several proteins would be affected, our results consistently point to a main role for the essential plasma membrane H^+-pump Pma1p in mediating the toxic effect of edelfosine, as well as of the clinically relevant ATLs miltefosine and perifosine. Pma1p is tightly associated with plasma membrane lipid rafts and this interaction is necessary for its ATPase activity (42) (Fig. 11a). Lipid rafts are highly compact microdomains enriched in ergosterol and sphingolipids and treatment with edelfosine disrupts these structures (Fig. 11a). Edelfosine and cholesterol have complementary conical geometries, which allow both molecules to bind tightly and form bilayers *in vitro* (43). It has been shown that edelfosine alters the organization of lipid rafts (44), and this biophysical change leads to alterations in the raft protein composition (4,12,17). This modification in raft organization is likely more extensive when sphingolipid (*FEN1*, *SUR4*) or ergosterol (*ERG3*) metabolic genes are deleted, these mutants being hypersensitive to edelfosine [Czyz *et al.* and (17)]. Once edelfosine alters lateral organization of the plasma membrane, Pma1p is displaced from rafts (17) followed by its internalization via endocytosis to late endosomes, and then eventually to the vacuole to be degraded (Fig. 11, b-c).

Through the use of radioactive and fluorescent edelfosine analogues we provide conclusive evidence that rules out the endocytic route for entrance of edelfosine into yeast. Our data suggest that edelfosine is internalized into the ER (Fig. 11d) through a non-endocytic pathway, but this intracellular location of the drug is not *per se* crucial for edelfosine toxicity in yeast. We interpret the retrieval from our edelfosine-resistance screen of mutants lacking components in several endocytic and trafficking pathways as a way to recycle Pma1p back to the plasma membrane. The model depicted in Fig. 11 implies that edelfosine treatment displaces Pma1p to the late endosome, and then eventually to the vacuole to be degraded. Our data suggest a putative mechanism of Pma1p degradation involving its ubiquitination (Fig. 11, $c_{(1)}$ and $c_{(2)}$), followed by recognition through the ESCRT complex (Fig. $11c_{(3)}$), a process highly conserved in eukaryotes, and then incorporation into MVB (Fig. $11c_{(4)}$), and subsequent degradation in the vacuole (Fig. $11c_{(5)}$). In endosome traffic-defective mutants, where the above mechanisms are not wholly functional, Pma1p could escape the endosome, preventing its entering the degradation pathway, and cycle back to the plasma membrane (Fig. 11, $c_{(6)}$ and $c_{(7)}$).

In support of this model, it has been described that a temperature-sensitive conditional mutant of *PMA1* (*pma1-7*, $Pma1p^{ts}$) undergoes growth arrest because newly synthesized protein is directed to the vacuole via endocytic intermediates at the restrictive temperature (45). Rerouting of this $Pma1p^{ts}$ mutant to the plasma membrane and a concomitant growth recovery could be achieved by inactivation of certain **s**uppressor **o**f ***p****ma1* (*SOP*) genes (44). Eight of these *SOP* mutants have defects in endosome-vacuole targeting of proteins. Interestingly, half of them [*vps29*Δ, *vps35*Δ (retromer), *vps27*Δ (ESCRT), *vps8*Δ (CORVET)] were also identified in our resistance screen to edelfosine. In *vps27*Δ and *vps8*Δ, traffic of an

inducible Pma1p^{ts} fused to GFP was monitored. It was demonstrated that these mutations blocked progress of the protein to the vacuole allowing its transport from the endosome to the plasma membrane (45). In this work we show similar results for *vps35*Δ and *vps29*Δ after treatment with edelfosine (Fig. 11, $c_{(6)}$ and $c_{(7)}$). Thus, the effect of edelfosine resembles that of the *pma1-7* mutant, with the difference in the case of edelfosine being that Pma1p reaches the endocytic compartment from the plasma membrane. A blockage in the trafficking pathway leading to the vacuole results in rerouting of Pma1p back to the plasma membrane overcoming the cytotoxic effect.

While it has been well documented recycling of proteins is enhanced in cells lacking ESCRT components, it is intriguing how lack of endosomal sorting function results in recycling of internalized Pma1p. We propose internalized Pma1p destined for degradation in the vacuole is scrutinized by the sorting machinery, ensuring it does not go back to the plasma membrane. Lack of sorting allows for diversion of internalized Pma1p to return to the plasma membrane. In this regard it is interesting to note that lack of the recently characterized sorting protein Ere1p (but not Ere2p), which is critical for recycling of the raft associated transporter Can1p (36), confers resistance to edelfosine (Supplementary Table S1). Targeting of membranes by the prototypic ATL edelfosine is unveiling a fascinating network of communication between plasma membrane and intracellular membranes, that rely on intracellular pH, to control cellular growth or death decisions.

ACKNOWLEDGEMENTS

We thank J. Kearley for technical assistance. This work was supported by grants from the Spanish Ministerio de Economia y Competitividad (SAF2005-04293, SAF2008-02251, SAF2011-30518), Red Temática de Investigación Cooperativa en Cáncer, Instituto de Salud Carlos III, cofunded by the Fondo Europeo de Desarrollo Regional of the European Union (RD06/0020/1037 and RD12/0036/0065), European Community's Seventh Framework Programme FP7-2007-2013 (grant HEALTH-F2-2011-256986, PANACREAS), Junta de Castilla y León (CSI052A11-2, CSI221A12-2) to F.M.; grants from the Spanish Ministerio de Economia y Competitividad (BIO2008-00194, BIO2011-23901) and Junta de Castilla y León (GR147) to J.L.R.; grants from the Fondo de Investigación Sanitaria and European Commission (FIS-FEDER 06/0813, PS09/01915) and Junta de Castilla y León (Biomedicine Project 2010-2011) to C.G.; grant from the Spanish Ministerio de Economia y Competitividad (CTQ2010-16457) to A.U.A.; grant CIHR 14124 to C.R.M.; and by an NSERC discovery grant, a URGC grant from the University of Calgary, and an NSERC UFA award to VZ. A.C.M. and V.H. were recipients of FPU predoctoral fellowships from the Spanish Ministerio de Ciencia e Innovación. C.G. was supported by the Ramón y Cajal Program from the Spanish Ministerio de Ciencia e Innovación.

References

1. Gajate, C., and Mollinedo, F. (2002) *Curr Drug Metab* **3**, 491-525.
2. Mollinedo, F., Gajate, C., Martin-Santamaria, S., and Gago, F. (2004) *Curr Med Chem* **11**, 3163-3184
3. Jendrossek, V., and Handrick, R. (2003) *Curr Med Chem Anti-Canc Agents* **3**, 343-353
4. Gajate, C., Del Canto-Jañez, E., Acuña, A. U., Amat-Guerri, F., Geijo, E., Santos-Beneit, A. M., Veldman, R. J., and Mollinedo, F. (2004) *J Exp Med* **200**, 353-365
5. Mollinedo, F., Fernandez-Luna, J. L., Gajate, C., Martin-Martin, B., Benito, A., Martinez-Dalmau, R., and Modolell, M. (1997) *Cancer Res* **57**, 1320-1328.
6. Gajate, C., Fonteriz, R. I., Cabaner, C., Alvarez-Noves, G., Alvarez-Rodriguez, Y., Modolell, M., and Mollinedo, F. (2000) *Int J Cancer* **85**, 674-682.
7. Gajate, C., and Mollinedo, F. (2007) *Blood* **109**, 711-719
8. Mollinedo, F., de la Iglesia-Vicente, J., Gajate, C., Estella-Hermoso de Mendoza, A., Villa-Pulgarin, J. A., Campanero, M. A., and Blanco-Prieto, M. J. (2010) *Oncogene* **29**, 3748-3757

9. Mollinedo, F., de la Iglesia-Vicente, J., Gajate, C., Estella-Hermoso de Mendoza, A., Villa-Pulgarin, J. A., de Frias, M., Roue, G., Gil, J., Colomer, D., Campanero, M. A., and Blanco-Prieto, M. J. (2010) *Clin Cancer Res* **16**, 2046-2054
10. Gajate, C., Matos-da-Silva, M., Dakir, EL-H., Fonteriz, R. I., Alvarez, J., and Mollinedo, F. (2012) *Oncogene* **31**, 2627-2639
11. van der Luit, A. H., Budde, M., Ruurs, P., Verheij, M., and van Blitterswijk, W. J. (2002) *J Biol Chem* **277**, 39541-39547.
12. Gajate, C., Gonzalez-Camacho, F., and Mollinedo, F. (2009) *PLoS ONE* **4**, e5044
13. Gajate, C., and Mollinedo, F. (2001) *Blood* **98**, 3860-3863.
14. Nieto-Miguel, T., Fonteriz, R. I., Vay, L., Gajate, C., Lopez-Hernandez, S., and Mollinedo, F. (2007) *Cancer Res* **67**, 10368-10378
15. Nieto-Miguel, T., Gajate, C., and Mollinedo, F. (2006) *J Biol Chem* **281**, 14833-14840
16. Mollinedo, F. (2007) *Expert Opin Ther Patents* **17**, 385-405
17. Zaremberg, V., Gajate, C., Cacharro, L. M., Mollinedo, F., and McMaster, C. R. (2005) *J Biol Chem* **280**, 38047-38058
18. Hanson, P. K., Malone, L., Birchmore, J. L., and Nichols, J. W. (2003) *J Biol Chem* **278**, 36041-36050
19. Bjornsti, M. A. (2002) *Cancer Cell* **2**, 267-273
20. Foury, F. (1997) *Gene* **195**, 1-10
21. Mager, W. H., and Winderickx, J. (2005) *Trends Pharmacol Sci* **26**, 265-273
22. Niedenthal, R. K., Riles, L., Johnston, M., and Hegemann, J. H. (1996) *Yeast* **12**, 773-786
23. Han, G. S., O'Hara, L., Carman, G. M., and Siniossoglou, S. (2008) *J Biol Chem* **283**, 20433-20442
24. Balguerie, A., Bagnat, M., Bonneu, M., Aigle, M., and Breton, A. M. (2002) *Eukaryotic cell* **1**, 1021-1031
25. Huh, W. K., Falvo, J. V., Gerke, L. C., Carroll, A. S., Howson, R. W., Weissman, J. S., and O'Shea, E. K. (2003) *Nature* **425**, 686-691
26. Ashburner, M., Ball, C. A., Blake, J. A., Botstein, D., Butler, H., Cherry, J. M., Davis, A. P., Dolinski, K., Dwight, S. S., Eppig, J. T., Harris, M. A., Hill, D. P., Issel-Tarver, L., Kasarskis, A., Lewis, S., Matese, J. C., Richardson, J. E., Ringwald, M., Rubin, G. M., and Sherlock, G. (2000) *Nat Genet* **25**, 25-29
27. Robinson, M. D., Grigull, J., Mohammad, N., and Hughes, T. R. (2002) *BMC bioinformatics* **3**, 35
28. Cherry, J. M., Adler, C., Ball, C., Chervitz, S. A., Dwight, S. S., Hester, E. T., Jia, Y., Juvik, G., Roe, T., Schroeder, M., Weng, S., and Botstein, D. (1998) *Nucleic Acids Res* **26**, 73-79
29. Quesada, E., Delgado, J., Gajate, C., Mollinedo, F., Acuña, A. U., and Amat-Guerri, F. (2004) *J Med Chem* **47**, 5333-5335
30. Mollinedo, F., Fernandez, M., Hornillos, V., Delgado, J., Amat-Guerri, F., Acuña, A. U., Nieto-Miguel, T., Villa-Pulgarin, J. A., Gonzalez-Garcia, C., Ceña, V., and Gajate, C. (2011) *Cell death & disease* **2**, e158
31. Pomorski, T., Lombardi, R., Riezman, H., Devaux, P. F., van Meer, G., and Holthuis, J. C. (2003) *Mol Biol Cell* **14**, 1240-1254
32. Riekhof, W. R., Wu, J., Gijon, M. A., Zarini, S., Murphy, R. C., and Voelker, D. R. (2007) *J Biol Chem* **282**, 36853-36861
33. Aouida, M., Page, N., Leduc, A., Peter, M., and Ramotar, D. (2004) *Cancer Res* **64**, 1102-1109
34. Aouida, M., Poulin, R., and Ramotar, D. (2010) *J Biol Chem* **285**, 6275-6284
35. Raths, S., Rohrer, J., Crausaz, F., and Riezman, H. (1993) *J Cell Biol* **120**, 55-65
36. Shi, Y., Stefan, C. J., Rue, S. M., Teis, D., and Emr, S. D. (2011) *Mol Biol Cell* **22**, 4093-4107
37. Seaman, M. N., McCaffery, J. M., and Emr, S. D. (1998) *J Cell Biol* **142**, 665-681
38. Hettema, E. H., Lewis, M. J., Black, M. W., and Pelham, H. R. (2003) *Embo J* **22**, 548-557
39. Rojas, R., van Vlijmen, T., Mardones, G. A., Prabhu, Y., Rojas, A. L., Mohammed, S., Heck, A. J., Raposo, G., van der Sluijs, P., and Bonifacino, J. S. (2008) *J Cell Biol* **183**, 513-526

40. Conibear, E., and Stevens, T. H. (2000) *Mol Biol Cell* **11**, 305-323
41. Katzmann, D. J., Babst, M., and Emr, S. D. (2001) *Cell* **106**, 145-155
42. Bagnat, M., Chang, A., and Simons, K. (2001) *Mol Biol Cell* **12**, 4129-4138
43. Busto, J. V., del Canto-Jañez, E., Goñi, F. M., Mollinedo, F., and Alonso, A. (2008) *J Chem Biol* **1**, 89-94
44. Ausili, A., Torrecillas, A., Aranda, F. J., Mollinedo, F., Gajate, C., Corbalan-Garcia, S., de Godos, A., and Gomez-Fernandez, J. C. (2008) *J Phys Chem B* **112**, 11643-11654
45. Luo, W., and Chang, A. (1997) *J Cell Biol* **138**, 731-746

FIGURE LEGENDS

Figure 1. Chemical structures of ATLs and edelfosine fluorescent analogues. Chemical structures of edelfosine (EDLF or ET), the related natural compound lysophosphatidylcholine (LysoPC), fluorescent edelfosine analogues PTE-ET, PTRI-ET, Et-BDP-ET and Yn-BDP-ET, and the ATLs miltefosine (MLTF), and perifosine (PRIF).

Figure 2. Edelfosine-resistant *S. cerevisiae* screen and mutants affecting drug uptake. (**a**) Toxicity threshold of two wild-type *S. cerevisiae* strains (haploid BY4741, diploid BY4743) and three single deletion mutants known to exert resistance to edelfosine following 48 h incubation. (**b**) Growth of the complete set of haploid *S. cerevisiae* yeast deletion mutants in the presence of 60 μM edelfosine (EDLF). Each dot (red, deletion mutant; blue, wild-type) represents the growth of each yeast strain in the presence of 60 μM edelfosine for 72 h. The dashed line delineates strains considered resistant to edelfosine. (**c**) Functional distribution of the 262 genes found to cause resistance to edelfosine when deleted. (**d**) Uptake of [^{3}H]edelfosine for three resistant strains found to have decreased drug incorporation relative to the wild-type (WT, black solid bar). Each pair of bars represents a single-gene deletion mutant (black patterned bar) alongside that mutant complemented by a centromeric plasmid carrying said gene (white patterned bar). Data shown are representative or mean values ± SD of at least three independent experiments.

Figure 3. Uptake of fluorescent analogues of edelfosine depends on *LEM3*. (**a**) Wild-type *S. cerevisiae* cells were incubated with the indicated fluorescent edelfosine compounds and imaged. (**b**) *lem3*Δ cells were incubated and imaged as above. Since little to no intracellular fluorescence was observed in *lem3*Δ cells, higher exposition times had to be used, which accounts for the increased noise. Images shown are from representative experiments repeated at least three times.

Figure 4. Localization pattern of different fluorescent analogues of edelfosine in the endoplasmic reticulum of *S. cerevisiae*. (**a**) PTE-ET localizes in the endoplasmic reticulum as shown by the organelle marker Elo3p tagged with GFP. (**b**) The same distribution pattern can be observed with PTRI-ET. (**c**,**d**) Et-BDP-ET and Yn-BDP-ET also localize in the endoplasmic reticulum as assessed by their visualization around the nucleolus marker Sik1p tagged with RFP and close to the vacuole, as seen by differential interference contrast (DIC).

Figure 5. Quantification of *S. cerevisiae* cells showing co-localization of PTE-ET with the ER markers Elo3p and Sec63p. (**a**) Cells carrying a Sec63-GFP (green fluorescence) bearing plasmid, as a marker for ER, were incubated with PTE-ET (pseudo-colored red) and imaged. Areas of co-localization between ER and PTE-ET in the merge panels are yellow. The corresponding light microscopy images are also shown. (**b**) Fluorescence microscopy images of PTE-ET and the ER markers Elo3p-GFP and Sec63p-GFP were examined, and stained cells were quantitated for the subcellular localization of the edelfosine fluorescent analogue. For each experiment, 150-300 stained cells were analyzed. Data shown are representative of mean values ± SD of at least three independent experiments.

Figure 6. Edelfosine and Pma1p subcellular localization following drug treatment. (**a**) Edelfosine fluorescent analogue PTE-ET colocalizes with the tagged ER marker protein Elo3p-GFP. (**b**) Influence of decreased endocytosis on drug uptake was assayed by comparing *end4 pep4*Δ cells (kept at the semi-permissive temperature of 25ºC) and wild-type cells switched to 4ºC with wild-type cells at 30ºC. Cells were incubated in the presence of the endocytic markers lucifer yellow (LY) and FM4-64, and afterwards with PTE-ET. (**c**) GFP-tagged Pma1p is internalized to the vacuole after edelfosine treatment (EDLF) at 30ºC; whereas at a temperature blocking endocytosis (4ºC), this process, unlike drug uptake (see panel **b**), is impaired. Images shown are from representative experiments repeated three times.

Figure 7. Edelfosine and Pma1p localization to lipid rafts following drug treatment of *S. cerevisiae*. Aliquots of sucrose gradient fractions for the isolation of lipid rafts from membrane-

enriched samples were analyzed for [^{3}H]edelfosine (**a**) and Pma1p (**b**) distribution. Adjoining figures represent fractions of the same samples. (**a**) [^{3}H]edelfosine distribution in fractions of wild-type cells after drug treatment for 15 min (WT 15 min) and 360 min (WT 360 min). Underlined fractions correspond to lipid rafts. Drug accumulation in lipid raft fractions is even more remarkable in drug-resistant *end 4pep4*Δ cells (*end4 pep4*Δ 360 min). *Inset*, Western blot of the raft protein Pma1p in untreated wild-type yeast (WT 0 min), identifying fractions 4-6 as raft-enriched fractions. The position of Pma1p is indicated by an arrow. (**b**) Pma1p (arrow) and Gas1p (arrowhead) distribution in sucrose gradient fractions obtained from the isolation of lipid rafts. Edelfosine alters Pma1p distribution relative to 15-min controls, decreasing its presence in lipid raft fractions. The resistant *end4 pep4*Δ strain manages to keep Pma1p in the edelfosine-enriched lipid rafts. Data shown are representative of three experiments performed.

Figure 8. Effect of ATLs on Pma1p localization following ATL treatment in *S. cerevisiae*. (**a**) Association of Pma1p with detergent-resistant membranes from wild-type yeast cells untreated (Control) or treated with 15 μM edelfosine (EDLF), 2.5 μM miltefosine (MLTF) or 3 μM perifosine (PRIF) for 2 h in defined medium. Lipid raft isolation was performed by using Optiprep gradients. (**b**) Percentages of Pma1p associated with fraction #2 (containing detergent-resistant membranes) were determined by densitometry using ImageJ. (**c**) Fluorescence microscopy of a yeast strain expressing Pma1-GFP untreated (Control) or treated with the indicated ATLs as above. Data shown are representative of three independent experiments performed.

Figure 9. Edelfosine resistance of *vps29*Δ and *vps35*Δ mutants. Growth curves of wild-type (BY4741), *vps29*Δ (*vps29*), *vps35*Δ (*vps35*) knock-out mutants and mutant strains harbouring the corresponding cognate genes (*vps29*-YCplac111-*VPS29* and *vps35*-YCplac111-*VPS35*) in SC medium containing 60 μM edelfosine. Data shown are mean values ± SD of at least six independent experiments.

Figure 10. Pma1p and edelfosine localization in wild-type *S. cerevisiae* and retromer mutants following drug addition. (**a**) Edelfosine-resistant retromer mutants *vps29*Δ and *vps35*Δ show the same pattern of ER localization as wild-type cells (WT) after treatment with PTE-ET. (**b**) Retromer mutants *vps17*Δ, *vps29*Δ and *vps35*Δ show decreased vacuolar accumulation of Pma1p-GFP relative to wild-type cells (WT) after edelfosine (EDLF) treatment, as shown by the vacuole-accumulating stain FM4-64. DIC, differential interference contrast. Data shown are representative of three independent experiments.

Figure 11. Proposed model for the mechanism of edelfosine cytotoxicity. (**a**) The essential proton pump Pma1p is associated with plasma membrane lipid rafts. (**b**) Edelfosine treatment causes the lipid raft to become disorganized. Edelfosine interacts with its core component ergosterol and Pma1p dissociates from the raft microdomains. (**c**) Edelfosine induces internalization and vacuole-dependent degradation of Pma1p. Deletion of ESCRT-complex genes causes resistance to edelfosine. Pma1p could thus be degraded by ubiquitination (1), internalization by endocytosis (2), recognition of ubiquitin moiety by the ESCRT complex (3), leading to recycling of the ubiquitin and enclosement of Pma1p in lumenal vesicles of the MVB (4). Fusion of the MVB with the vacuole would lead to degradation of these Pma1p-containing vesicles (5). Vacuolar hydrolases could also degrade Pma1p. The retromer complex is essential for the effect of the drug. We postulate this complex is either withdrawing Pma1p from the endosome to the Golgi apparatus (GA) via retrograde transport (6), or allowing the delivery of lysosomal hydrolases essential for the degradation of Pma1p (not shown). If any of these degradation pathways are impaired, a greater quantity of Pma1p could be available for recycling to the plasma membrane (7). (**d**) Both ergosterol and edelfosine are internalized. The drug accumulates in the endoplasmic reticulum (ER), and in some hitherto uncharacterized compartment in the cytoplasm. (**e**) pH homeostasis in physiological conditions is tightly controlled by Pma1p-mediated proton extrusion, V-ATPase proton sequestering, and mitochondria-mediated proton pumping. Edelfosine decreases the availability of the first buffering mechanism, causing acidification. When edelfosine is added to cells lacking a functional V-ATPase,

the loss of functional Pma1p leads to a greater cytosolic acidification resulting in hypersensitivity to the drug.

Table 1. Yeast strains and plasmids used in this study.

Strain	Genotype	Reference
BY4741	*MATa his3Δ1 leu2Δ0 met15Δ0 ura3Δ0*	Euroscarf
BY4742	*MATα his3Δ1 leu2Δ0 lys2Δ0 ura3Δ0*	Euroscarf
BY4743	*MATa/α his3Δ1/his3Δ1 leu2Δ0/leu2Δ0 LYS2/lys2Δ0 met15Δ0/MET15 ura3Δ0/ura3Δ0*	Euroscarf
S288C	*MATα his3Δ1 leu2Δ0 lys2Δ0 ura3Δ0*	ATCC 201389
ERG6-RFP	*ERG6::RFP kanMX4* derivative of S288C	P. Arvidson (25)
PEX3-RFP	*PEX3::RFP kanMX4* derivative of S288C	P. Arvidson (25)
ANP1-RFP	*ANP1::RFP kanMX4* derivative of S288C	P. Arvidson (25)
SPC42-RFP	*SPC42::RFP kanMX4* derivative of S288C	P. Arvidson (25)
SNF7-RFP	*SNF7::RFP kanMX4* derivative of S288C	P. Arvidson (25)
SAC6-RFP	*SAC6::RFP kanMX4* derivative of S288C	P. Arvidson (25)
CHC1-RFP	*CHC1::RFP kanMX4* derivative of S288C	P. Arvidson (25)
RH1800	*MATa leu2 his4 ura3-52 bar1*	H. Riezman (17)
RH2763	*MATa his4 leu2 ura3 bar1 pep4::URA3 sla2-1 (end4^{ts})*	H. Riezman (17)

Table 2. Relevant genes involved in edelfosine-induced yeast toxicity. Resistant mutants were identified from chemical-genomic screens of the *S. cerevisiae* deletion mutant collection.

Functional categories associated with edelfosine-resistance analyzed in this study					
Drug uptake	**Vesicular traffic**				
	Endocytosis	ESCRT complexes		Retrograde transport	
		Complex 0	Complex III related	Retromer	GARP complex
DRS2	*END3*	*VPS27*	*DID2*	*VPS17*	*VPS52*
DNF2	*MYO5*		*VPS4*	*VPS26/PEP8*	*VPS54*
LEM3	*RHO4*	Complex I		*VPS29*	
AGP2	*LDB17*	*VPS23/STP22*	Associated components	*VPS35*	Others
DOC1		*VPS37/SRN2*	*BRO1*	CORVET	*GYP6*
		Complex III	*DOA4*	*VPS3*	*SNX4*
		DID4/VPS2	*UBP2*	*VPS8*	*SNX42*
		VPS24			*CCZ1*
		VPS20			*YPT7*
					TLG2
					SWF1
					KEX1
					KEX2

Figure 1, Cuesta-Marbán *et al.*

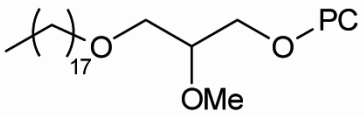

edelfosine (EDLF or ET)

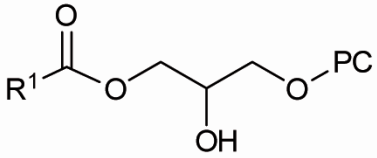

LysoPC (R^1 = acyl group chain)

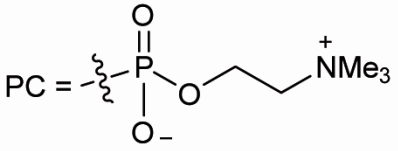

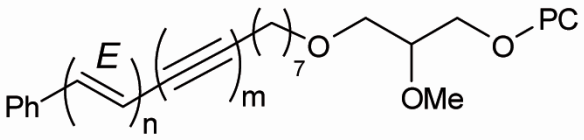

PTE-ET: n = 4, m = 0

PTRI-ET: n = 3, m = 1

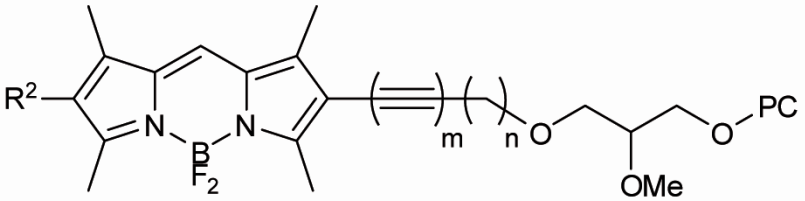

Et-BDP-ET: R^2 = Et, n = 11, m = 0

Yn-BDP-ET: R^2 = H, n = 9, m = 1

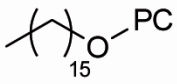

miltefosine (MLTF)

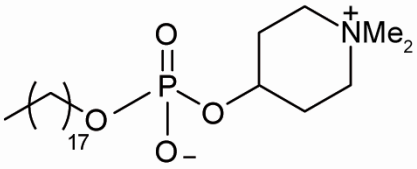

perifosine (PRIF)

Figure 2, Cuesta-Marbán *et al.*

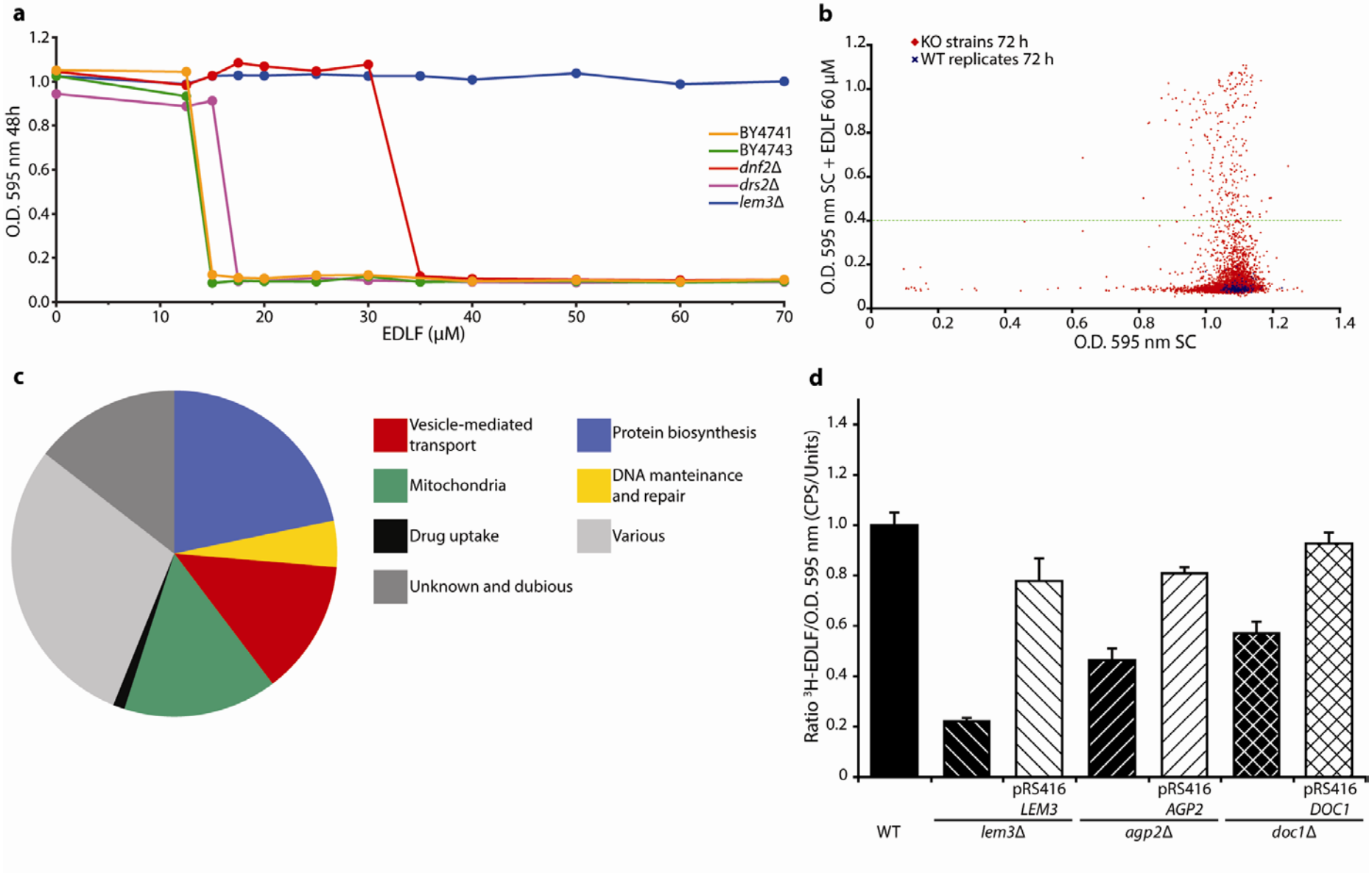

Figure 3, Cuesta-Marbán *et al.*

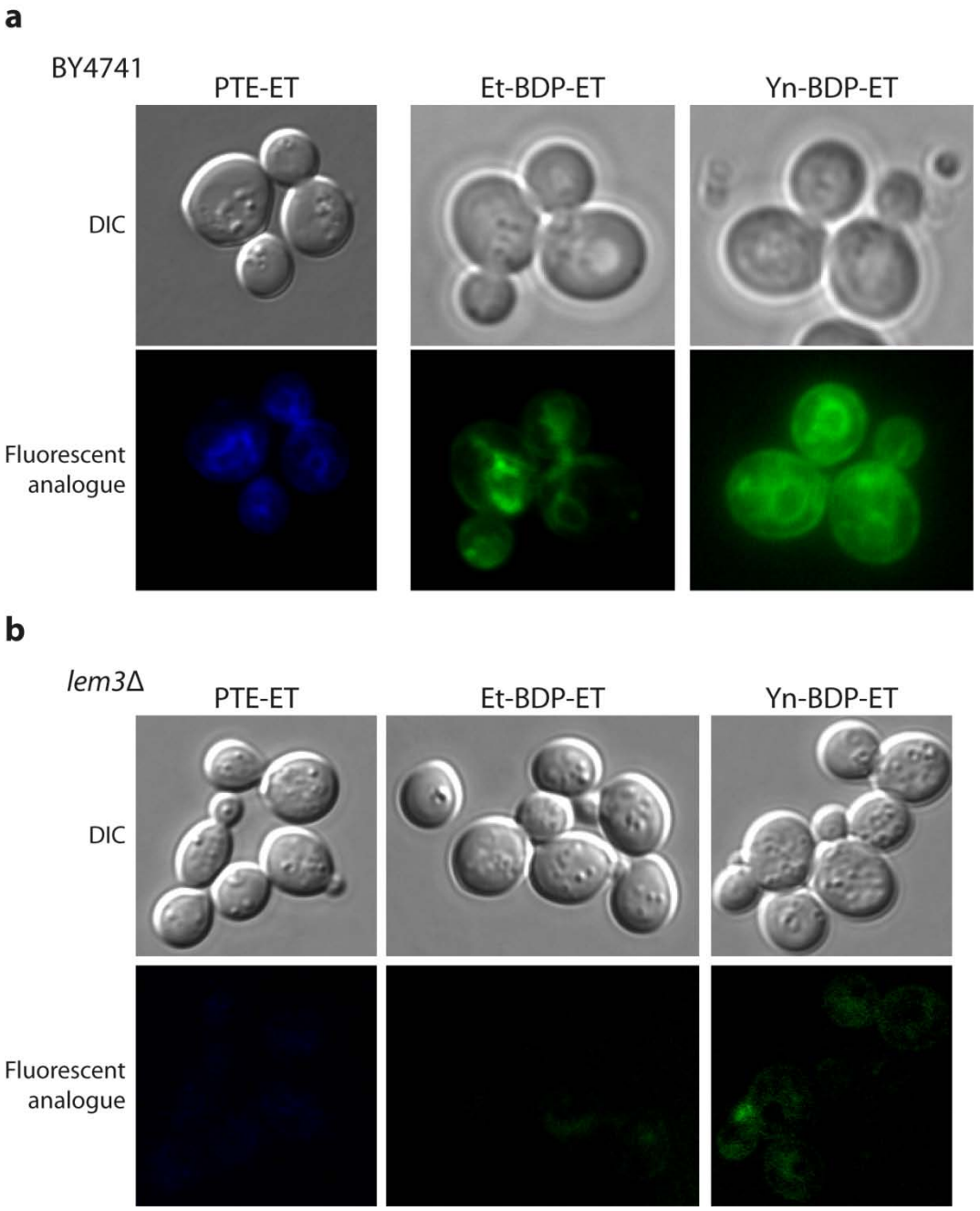

Figure 4, Cuesta-Marbán *et al.*

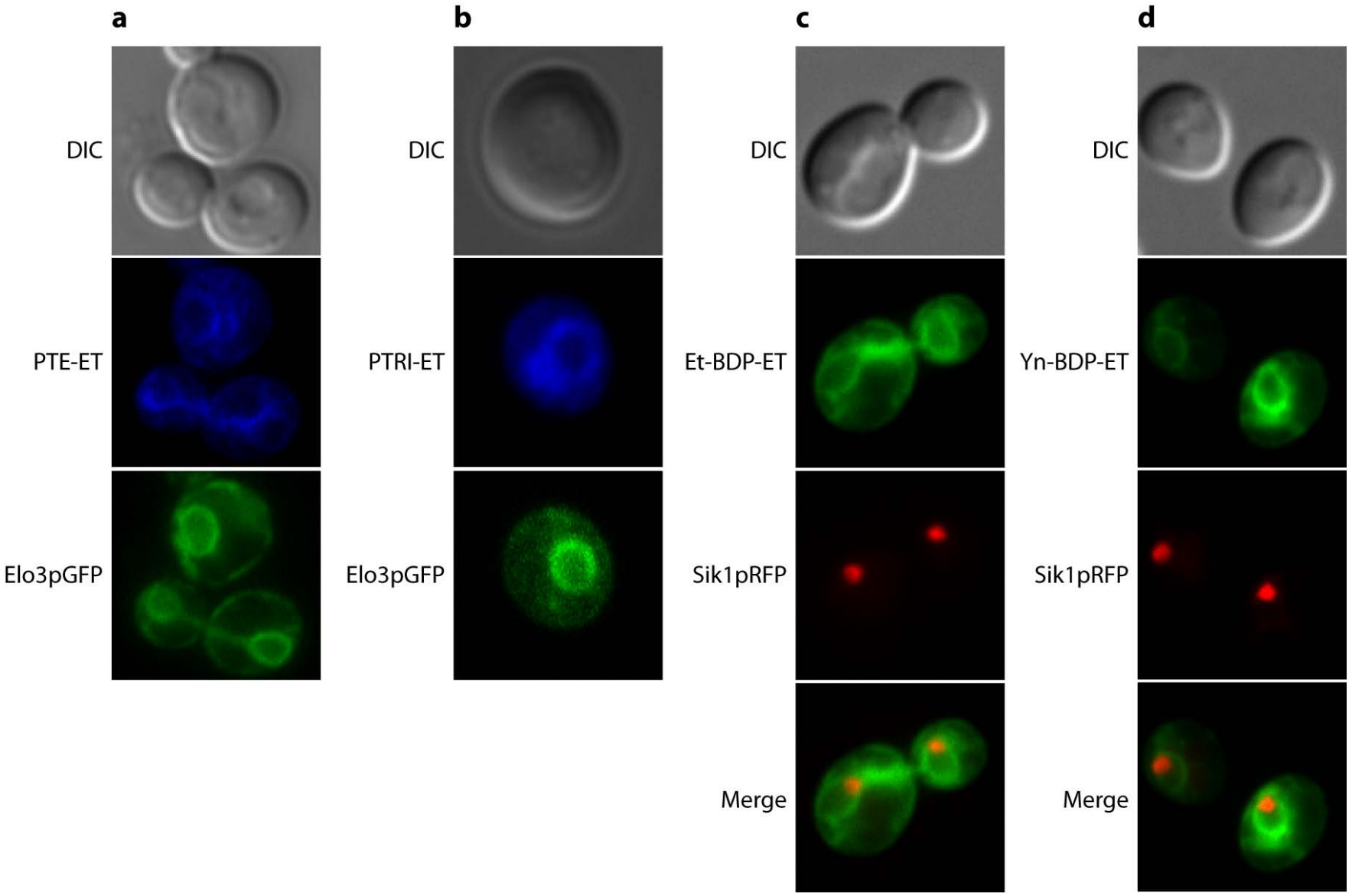

Figure 5, Cuesta-Marbán *et al.*

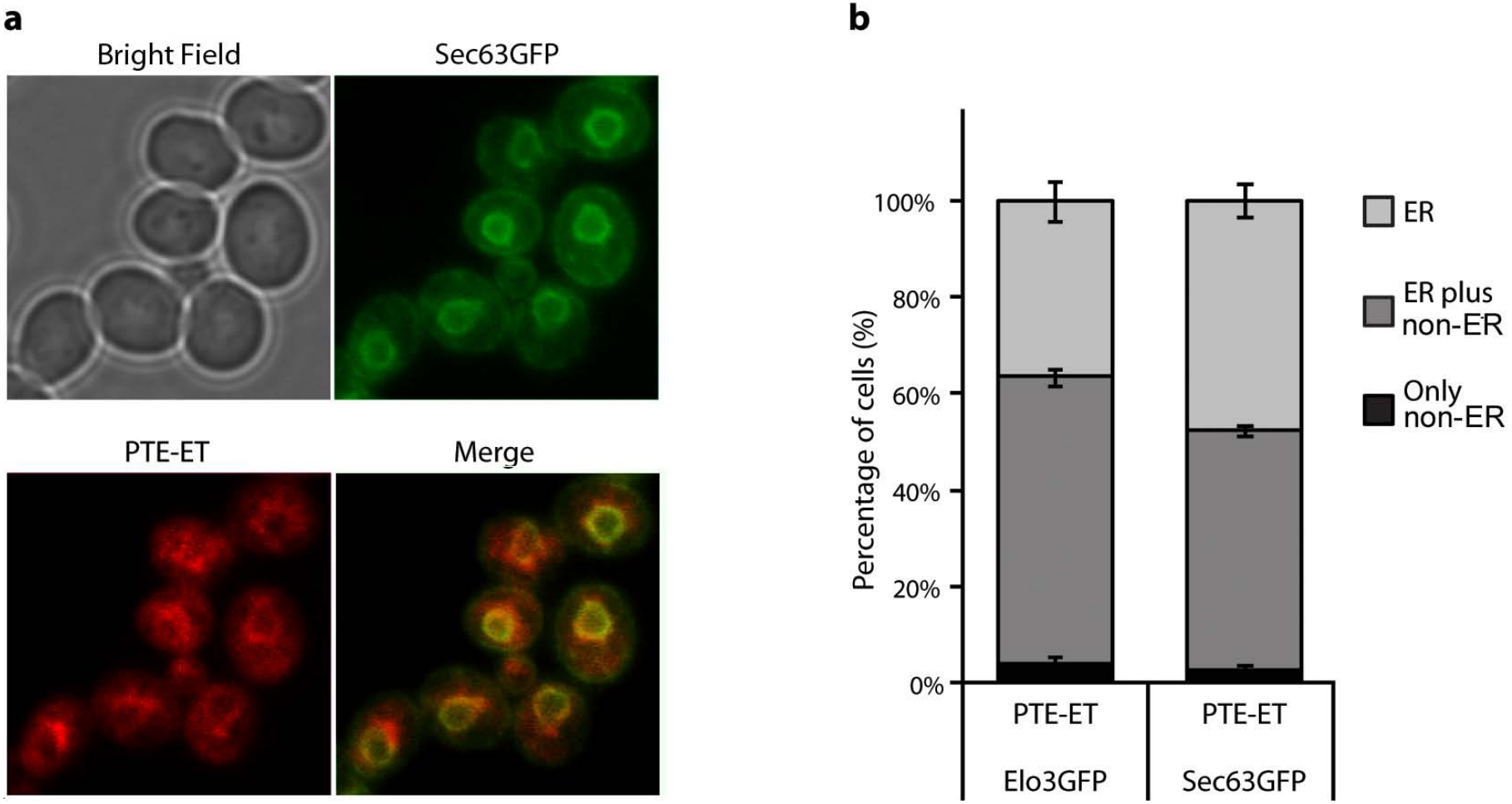

Figure 6, Cuesta-Marbán *et al.*

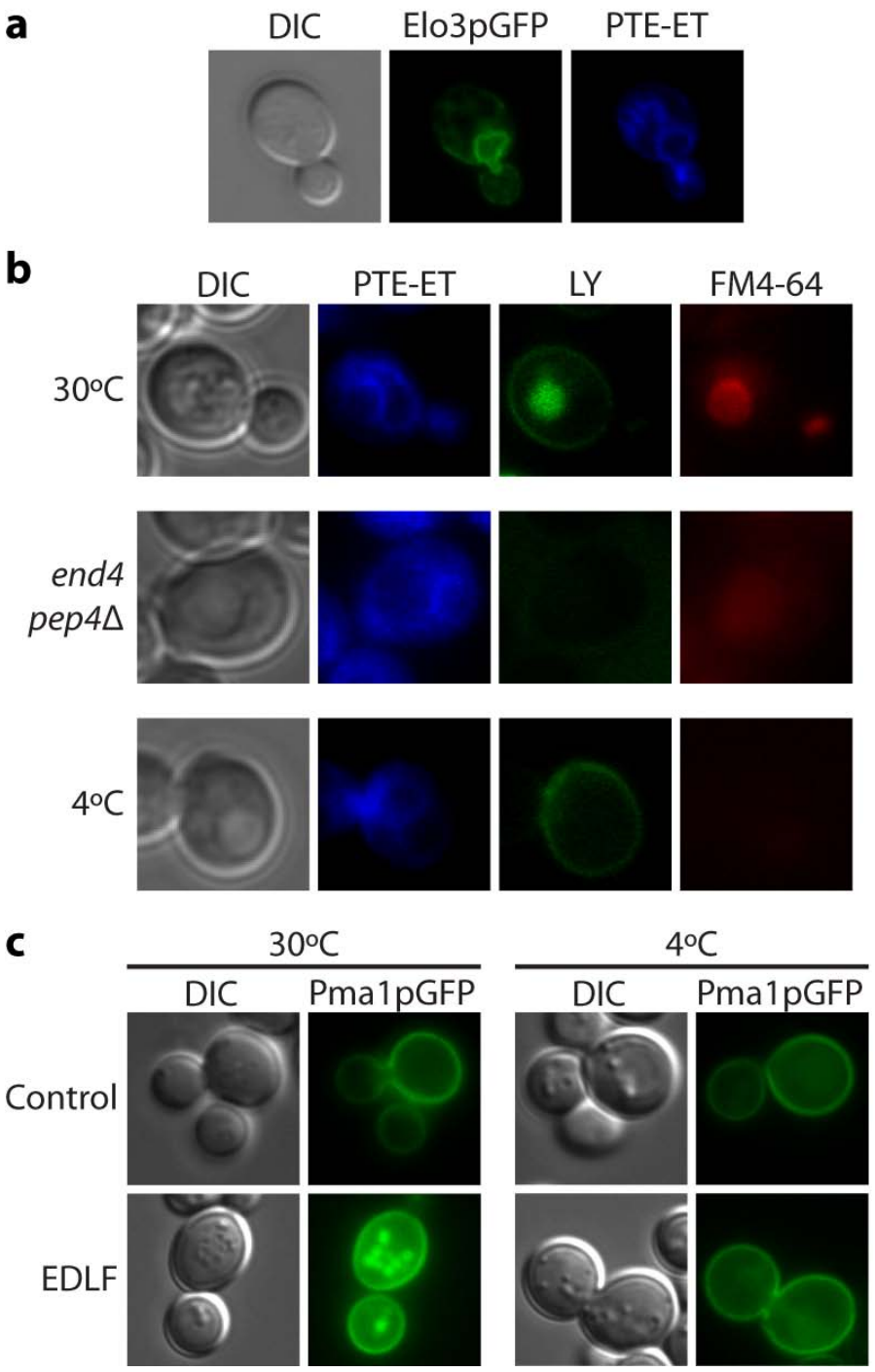

Figure 7, Cuesta-Marbán *et al.*

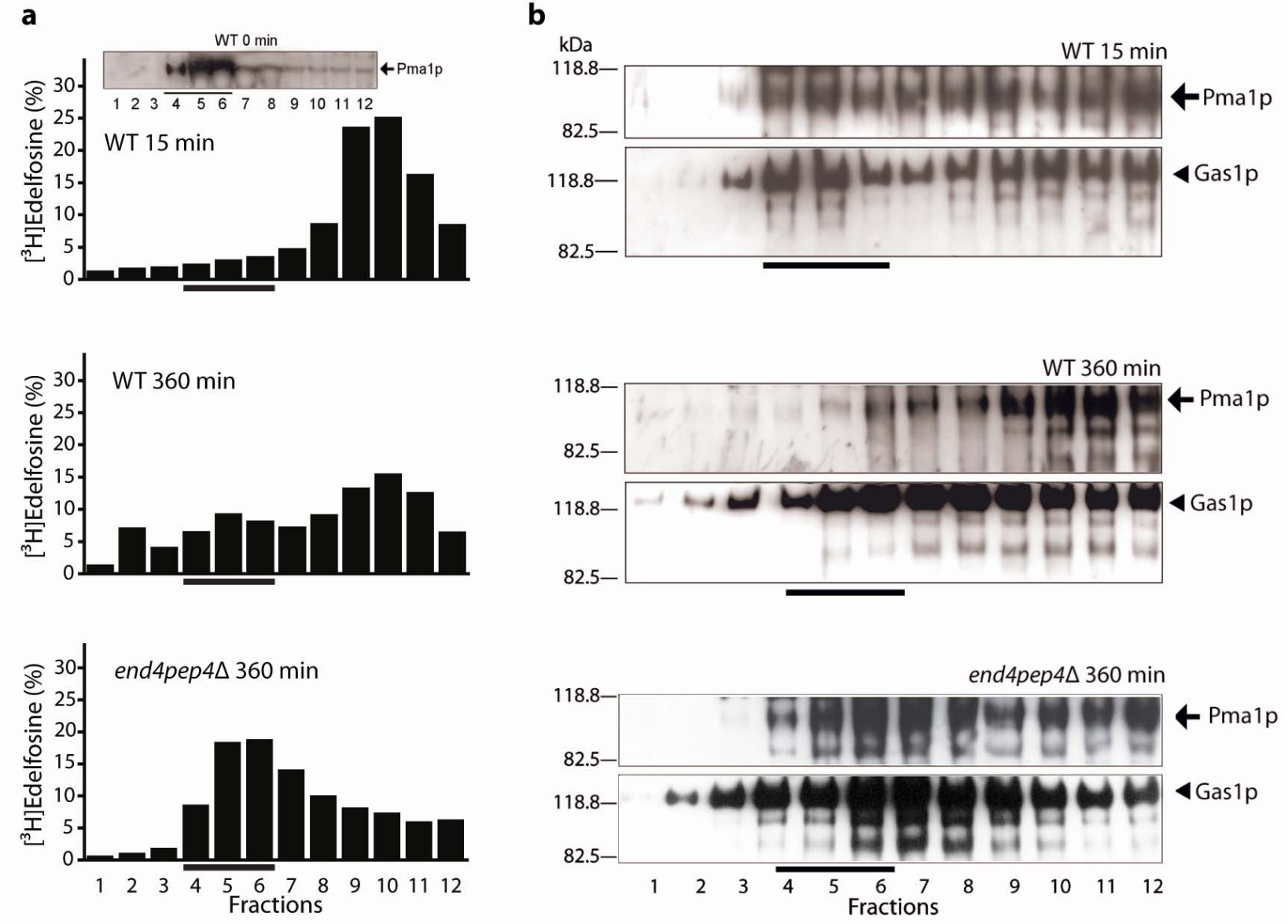

Figure 8, Cuesta-Marbán *et al.*

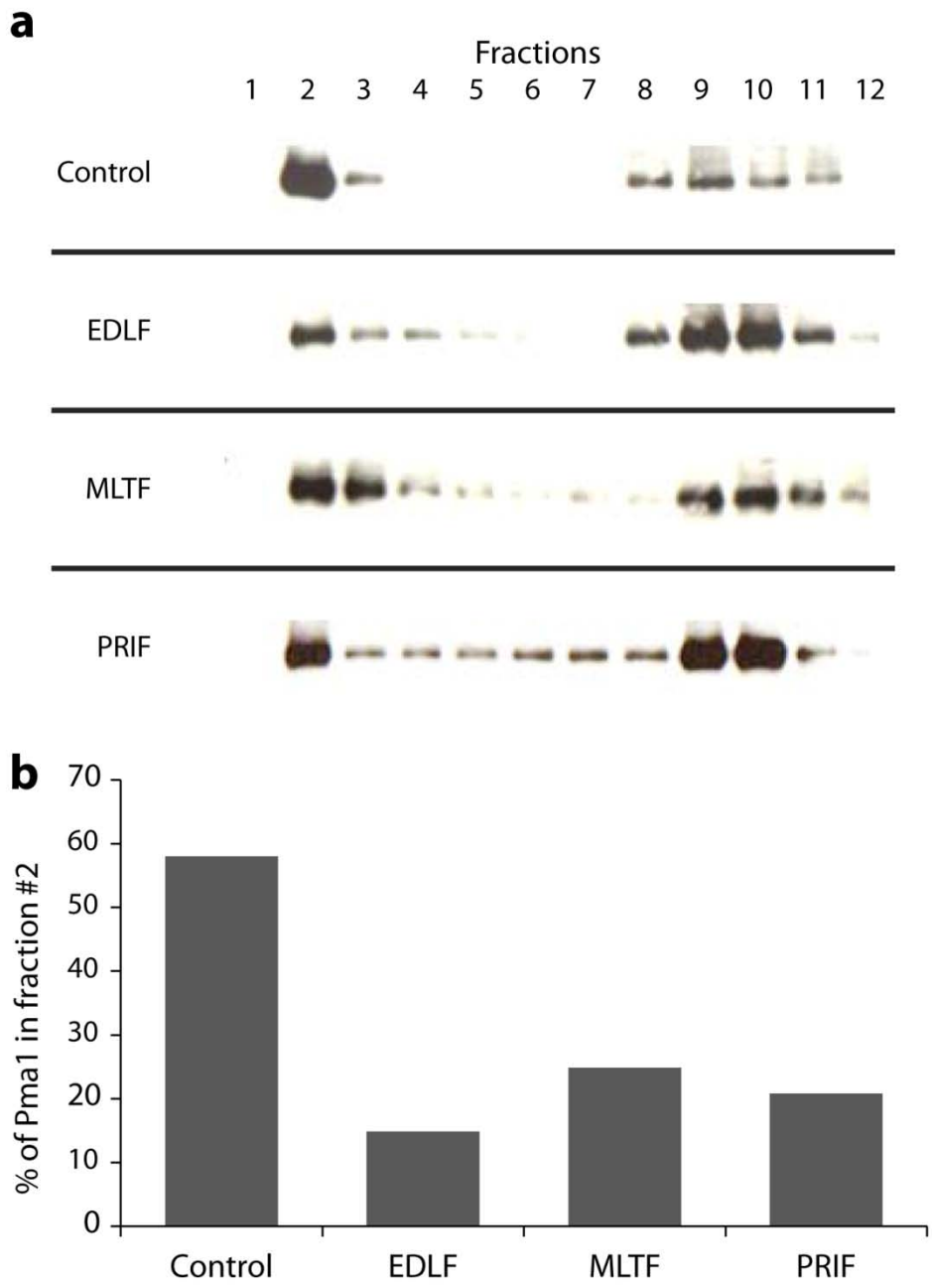

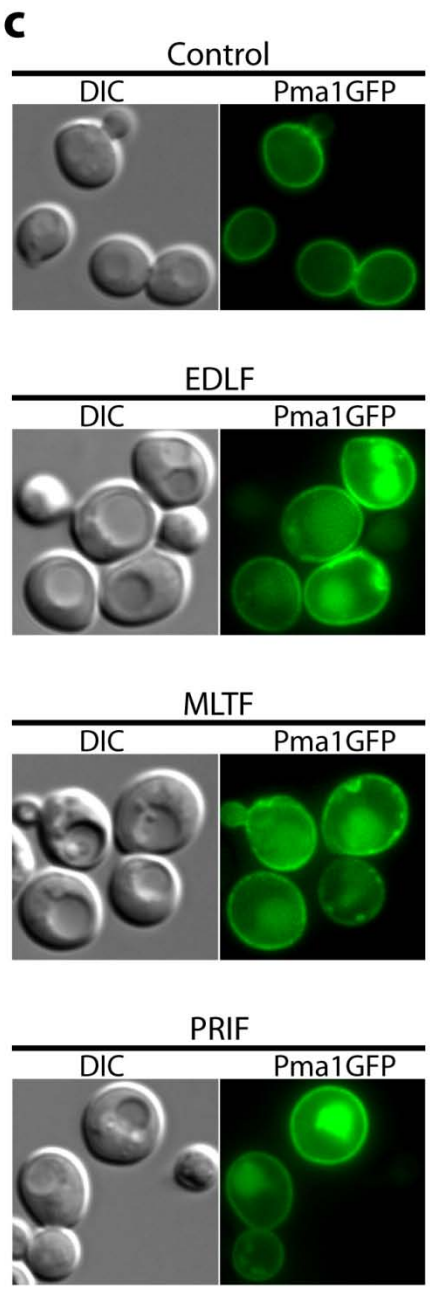

Figure 9, Cuesta-Marbán *et al.*

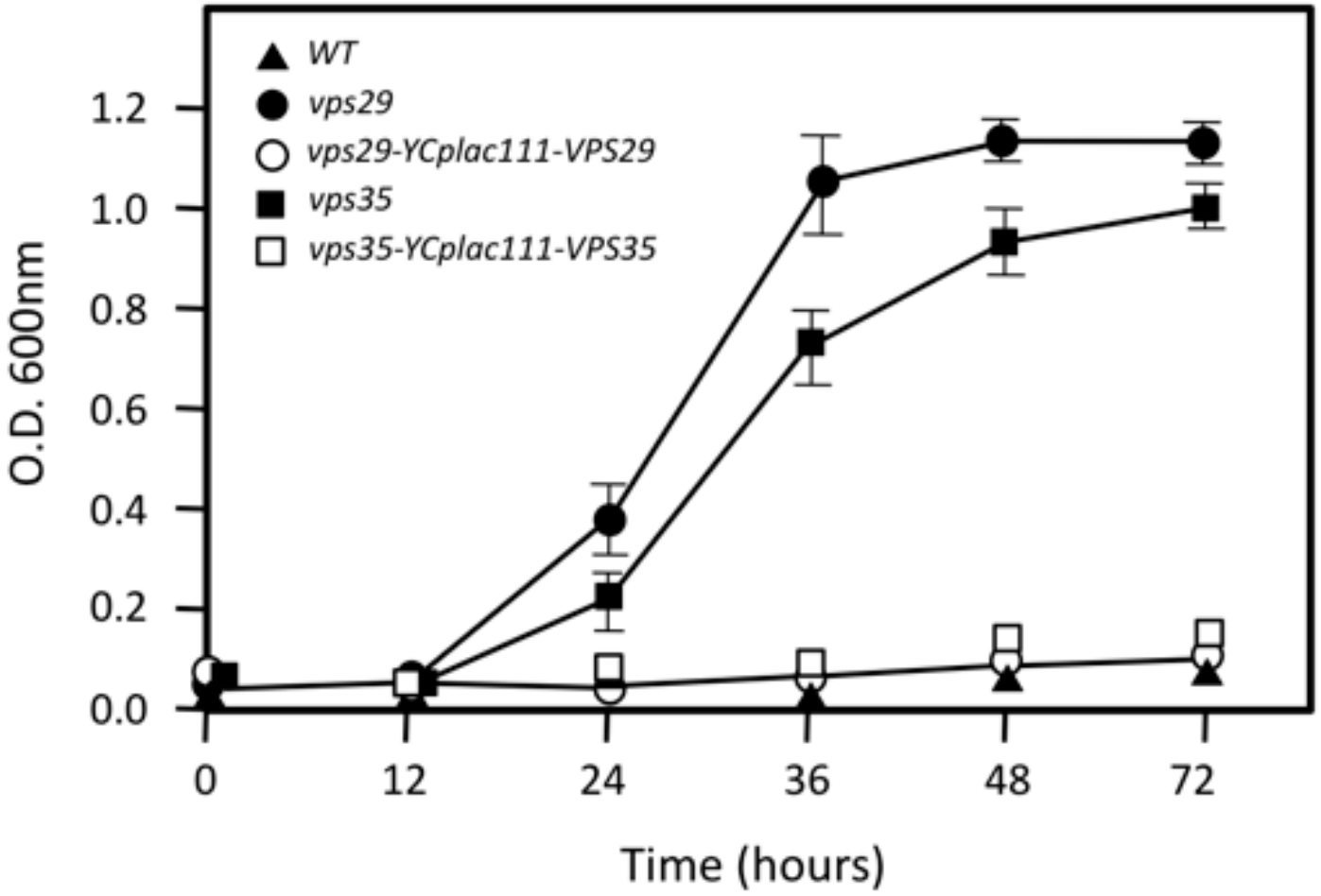

Figure 10, Cuesta-Marbán *et al.*

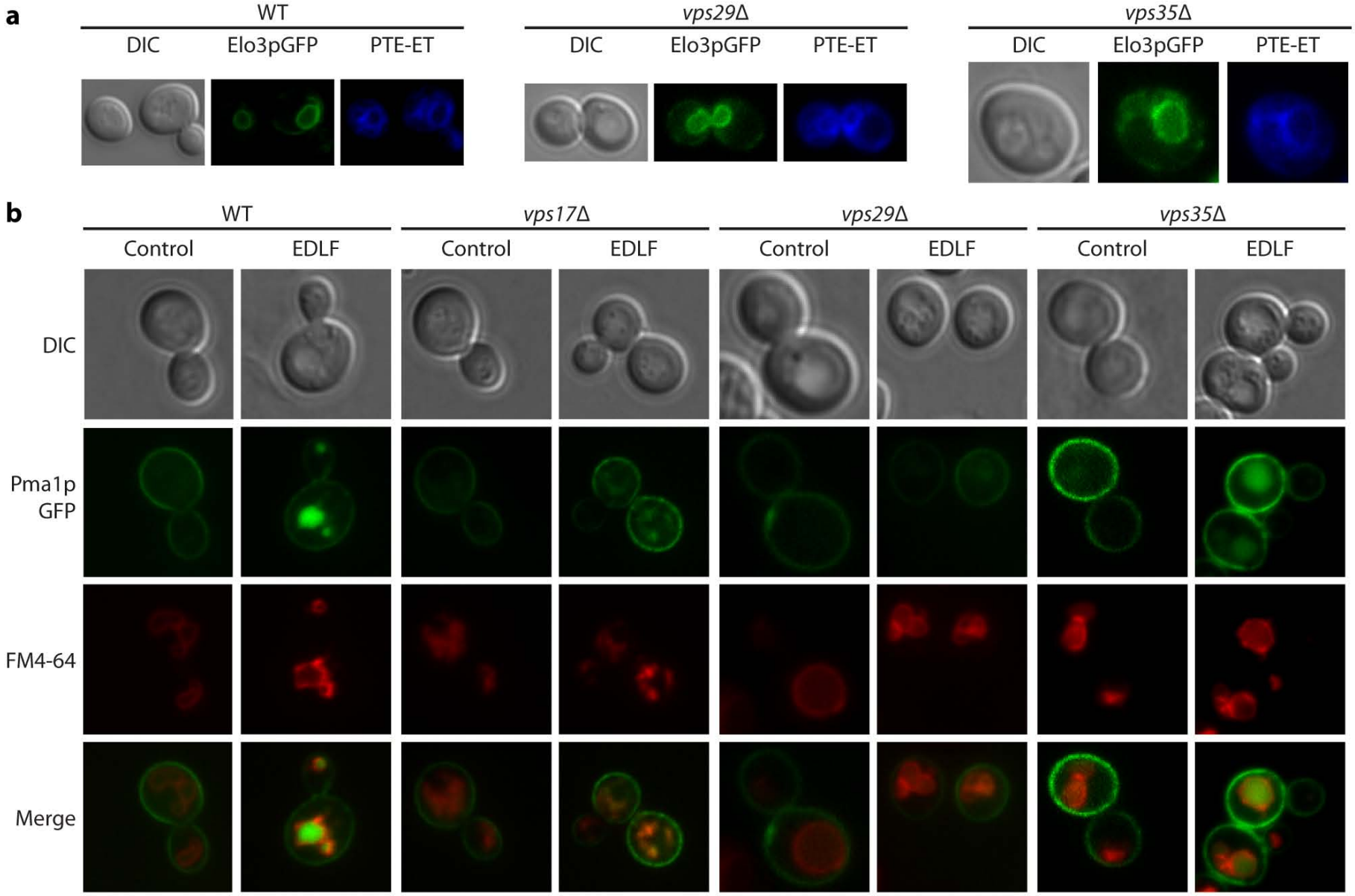

Figure 11, Cuesta-Marbán *et al.*